

ORIGINAL INNOVATION

Open Access



# Probabilistic seismic response analysis of coastal highway bridges under scour and liquefaction conditions: does the hydrodynamic effect matter?

Xiaowei Wang<sup>1,2</sup> , Yutao Pang<sup>3\*</sup> and Aijun Ye<sup>4</sup>

\* Correspondence: [pangyutao@cug.edu.cn](mailto:pangyutao@cug.edu.cn)

<sup>3</sup>Faculty of Engineering, China University of Geosciences (Wuhan), Wuhan 430074, Hubei, China  
Full list of author information is available at the end of the article

## Abstract

Coastal highway bridges are usually supported by pile foundations that are submerged in water and embedded into saturated soils. Such sites have been reported susceptible to scour hazard and probably liquefied under strong earthquakes. Existing studies on seismic response analyses of such bridges often ignore the influence of water-induced hydrodynamic effect. This study assesses quantitative impacts of the hydrodynamic effect on seismic responses of coastal highway bridges under scour and liquefaction potential in a probabilistic manner. A coupled soil-bridge finite element model that represents typical coastal highway bridges is excited by two sets of ground motion records that represent two seismic design levels (i.e., low versus high in terms of 10%-50 years versus 2%-50 years). Modeled by the added mass method, the hydrodynamic effect on responses of bridge key components including the bearing deformation, column curvature, and pile curvature is systematically quantified for scenarios with and without liquefaction across different scour depths. It is found that the influence of hydrodynamic effect becomes more noticeable with the increase of scour depths. Nevertheless, it has minor influence on the bearing deformation and column curvature (i.e., percentage changes of the responses are within 5%), regardless of the liquefiable or nonliquefiable scenario under the low or high seismic design level. As for the pile curvature, the hydrodynamic effect under the low seismic design level may remarkably increase the response by as large as 15%–20%, whereas under the high seismic design level, it has ignorable influence on the pile curvature.

**Keywords:** Coastal bridge, Probabilistic seismic response, Hydrodynamic effect, Scour, Liquefaction

## 1 Introduction

Coastal highway bridges have been increasingly constructed as rapid transportation pathways for the development urban communities. Such kinds of bridges are normally supported by substructure systems consisting of column and pile-foundation that penetrate through water and into soils. Under such site and environmental conditions, seismic excitations-induced dynamic behavior of water and soils is expected to influence seismic responses of the bridges. The water-related influence is normally called the hydrodynamic effect (Westergaard 1933; Liaw and Chopra 1974; Goyal and Chopra 1989), while the soil-related influence may trigger liquefaction consequences when saturated cohesionless soils are involved in the site soil profiles (Aygün et al. 2011; Wang et al. 2019b). In addition to the seismic hazard, scour has been reported as another common hazard to coastal bridges due to the intensifying climate changes (Khelifa et al. 2013; Yang and Frangopol 2019). In this regard, the seismic behavior of coastal highway bridges under the combined effects of scour, liquefaction, and hydrodynamics are worth for investigation.

Although enormous studies on seismic responses of bridges under the scour hazard have been reported in the past decade (Alipour et al. 2012; Wang et al. 2014; Guo et al. 2016; Fioklou and Alipour 2019; Liu et al. 2020; Song et al. 2020; Liang et al. 2020, among others), none of them included the hydrodynamic effect to the best knowledge of the authors. Instead, the hydrodynamic effect is often separately considered in seismic analyses of bridges (e.g., Wei et al. 2013; Li and Yang 2013; Jiang et al. 2017; Wang et al. 2019; Zhang et al. 2019; Pang et al. 2015, 2020; Zhang et al. 2020b). For this reason, the influence of hydrodynamic effect on the seismic responses of bridges under different scour depths is yet to be well quantified. On the other hand, despite insights on seismic response characteristics of bridges in liquefiable soils have been significantly advanced in the past decade (Padgett et al. 2010; Aygün et al. 2011; Brandenberg et al. 2011; Cubrinovski et al. 2014; Khosravifar et al. 2014a; Mohanty et al. 2017; Wang et al. 2017a; Xie et al. 2018; Zhang et al. 2020a, among others), very few studies considered the combined effects of liquefaction and scour (Wang et al. 2019c, 2020) or the combined effects of liquefaction and hydrodynamics (Robertson et al. 2007; Padgett et al. 2012). In other words, the hydrodynamic effect is usually ignored in the seismic analyses of bridges under scour or liquefaction. However, as these environmental effects are susceptible to occur simultaneously and may interplay with each other (Wang et al. 2019c), it is of particular importance to examine the quantitative influence of the hydrodynamic effect on seismic responses of coastal highway bridges under scour and liquefaction potential. This noted research gap motivates the present study.

The objective of this paper is to quantify the influence of hydrodynamic effect on seismic responses of coastal highway bridges under scour and liquefaction potential. First, a typical coastal highway bridge at an earthquake-prone region of China is adopted and modeled based on experimentally validated numerical modeling methods. After that, the quantitative influence of the hydrodynamic effect on the responses of bridge key components (e.g., bearing deformation, column curvature, and pile curvature) are probabilistically assessed considering liquefiable and nonliquefiable scenarios, both with scour depths from 0 to 6 m, under two seismic design levels that are commonly considered in seismic design practices (i.e., 10%-50 years and 2%-50 years). Finally, conclusions and future studies are addressed, together with the limitations.

## 2 Numerical modeling and ground motions

### 2.1 Scope of studied coastal bridges

The studied coastal bridges are limited to the widely constructed multi-span highway bridges along coastlines, as indicatively shown in Fig. 1, an along-sea highway bridge at southeast coastal region of China. Individual bents of these bridges are commonly supported by reinforced concrete (RC) columns through elastomeric rubber bearings. The RC columns are supported by rigid RC caps connecting pile-group foundations submerged in water and embedded into soils that may be subjected to scour and liquefaction under earthquakes. As the individual bents normally have fairly close properties of strength and stiffness, seismic responses of the bridge can be approximately characterized by one bent. This simplified modeling strategy has been utilized by several other researchers as well as in the former studies of the authors (Hutchinson et al. 2004; Khosravifar et al. 2014b; Wang et al. 2018, 2019a). In light of engineering practices, the studied bent represents a typical coastal highway bridge with a single circular column (height of 6.5 m, diameter of  $D = 2$  m, and axial load ratio of  $\alpha = 10\%$ ), supported by a cuboid cap (length $\times$ width $\times$ height of  $L \times W \times H = 7.5 \times 5.5 \times 2.8$  m) on top of a  $2 \times 3$  pile-group (pile diameter of  $d = 1$  m and center-to-center distance of  $3d$ ) submerged in water and embedded into layered cohesionless soil profiles (an 8 m-thickness loose sand layer with a relative density of  $D_r = 37\%$  overlying a 22 m-thickness dense sand layer with  $D_r = 75\%$ ). Two scenarios soil profiles, i.e., liquefiable versus nonliquefiable, are considered. Besides, it is assumed that the original mud line is just below the cuboid cap. Multiple scour depths from 0 m to 6 m, at a space of 1 m, are considered to cover the possible range in engineering practices (Alipour et al. 2012).

### 2.2 Multi-dimensional coupled soil-bridge model

A multi-dimensional coupled soil-bridge model of the considered bent is established in the open-source finite element platform, OpenSEES (McKenna et al. 2010). The finite element model is composed by a two-dimensional (2D), three-degree-of-freedom

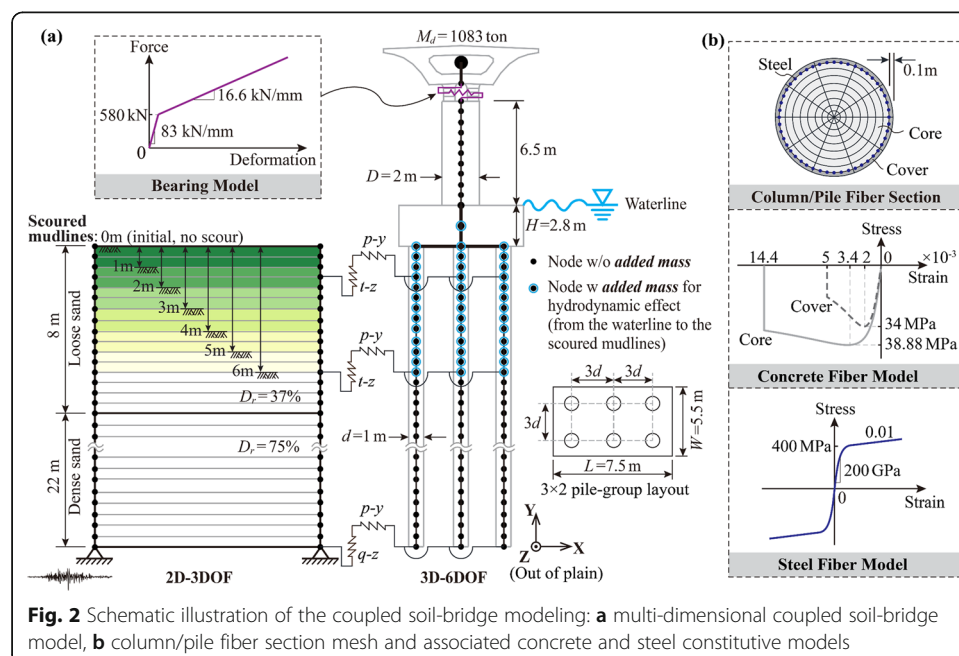


**Fig. 1** A typical multi-span coastal bridge at southeast coastal region of China

(3DOF) soil domain linking to 3D-6DOF structural domain through horizontally and vertically uniaxial soil-pile springs, as illustrated in Fig. 2. The purpose of multi-dimensional modeling is to save computational time in the analysis of soil behavior while maintaining accuracy in the analysis of bridge behavior. Translationally fixed constraints are assigned at the bottom of the soil domain, where seismic excitations are imposed. Each pair of soil nodes at the same depth is tied to achieve the shear behavior of the soil profile under horizontal excitations.

The deck is represented by a lumped mass,  $M_d$ , calculated by the column properties (i.e., concrete strength,  $f_c = 34$  MPa, gross section area,  $A_g = \pi \cdot 2^2 / 4 = 3.14$  m<sup>2</sup>, and axial load ratio,  $\alpha = 10\%$ , resulting in  $M_d = \alpha \cdot f_c \cdot A_g / g = 1083$  ton). The bilinear constitutive model by Zhang and Huo (2009) is adopted to represent the elastomeric rubber bearing. The column and piles are simulated using displacement-based beam-column elements with fiber sections (Fig. 2b); each element has a length of 0.5 m with five integration points (He et al. 2016). The fiber section is meshed to have one and eight segments in the radial direction for concrete cover and core, respectively, and ten segments in the circular direction. Similar meshes have been utilized in recent studies on inelastic seismic responses of bridges (e.g., Zhong et al. 2019, 2020; Chen 2020). In the fiber sections, the steel fibers are represented by the bilinear model with a smooth transition (Filippou et al. 1983), i.e., Steel02 material, while the concrete cover and core fibers are represented by Mander et al. (1988), i.e., Concrete04 material. The Concrete04 material parameters of the concrete core are calculated following Mander et al. (1988) based on longitudinal and transverse reinforcement ratios of 2% and 1%, respectively. The cuboid cap is modeled using rigid elements with a lumped mass of 300 ton.

Four-node QuadUP shear-beam elements, which can simulate solid–fluid responses under cyclic loads (Biot 1955), are used to represent the soil profiles based on the pressure-dependent-multi-yield material model (Yang 2000). The soil elements are meshed into 0.5 m to ensure the reasonable propagation of seismic waves (Zhang et al. 2008).



The soil-pile interaction is modeled by zero-length  $p$ - $y$ ,  $t$ - $z$ , and  $q$ - $z$  springs for the lateral, friction, and pile-tip vertical resistance, respectively (Boulanger et al. 1999; Brandenberg et al. 2013). A  $p$ -multiplier of 0.8 is adopted to account for the pile-group effect for the pile center-to-center distance of  $3d$  (Mokwa 1999). The soil constitutive model parameters are determined based on their relative densities following tabulated calculation process in Wang et al. (Wang et al. 2017b; Wang et al. 2019b). In particular, soil permeability coefficients in the liquefiable scenario are calculated as  $1.24 \times 10^{-4}$  m/s and  $7.94 \times 10^{-5}$  m/s for the loose and dense sand layers, respectively, whereas in the nonliquefiable scenario, a very large permeability coefficient of 1.0 m/s is taken to mitigate the liquefaction potential (Su et al. 2017). Note that the above-described numerical modeling technique has been experimentally validated using a series of centrifuge tests. For conciseness, details of the validation refer to Wang et al. (2017b). The above model is taken as the reference case without the hydrodynamic effect, while the modeling of hydrodynamic effect and associated validation are described in a separate section below, for legibility.

### 2.3 Modeling of hydrodynamic effect

The hydrodynamic effect is concerned with the water pressures acting on the structure, which could cause additional dynamic forces and modify the dynamic properties of the structure (Westergaard 1933). There are two main methods for the simulation of the hydrodynamic effect on structures. One is the analytical or simplified numerical method with “added mass” representing the water moving with the structures (Morison et al. 1950; Liaw and Chopra 1974; Bhatta and Rahman 2003). The other is the sophisticated numerical method with coupled fluid-structure interaction (Olson and Bathe 1985; Di Pilato et al. 2008; Wei et al. 2013). Each method has merits and demerits in terms of application scopes, simulation accuracy, and computational efficiency (Wei et al. 2013; Zhang et al. 2020a, 2020b). The former is apparently computational efficient, but special attention should be paid to the calculation of added mass that significantly affects the accuracy of the method. The latter excels in the simulation of complex fluid-structure interaction involving, for example, tsunami or storm surge-induced breaking waves. However, it often requires huge computational costs and perhaps numerical convergence issues would occur when structural nonlinear behavior is considered in particular. As the studied bridge is not supposed to suffer extreme hydrodynamic loads such as the breaking waves, as well as towards the balance of accuracy and computational efficiency, the hydrodynamic effect in the present study is modeled using the well-known added mass method, which has been validated experimentally and numerically by the authors (Pang et al. 2015, 2020). For clarification, the calculation process for the added mass is interpreted below.

For piles with circular cross-sections, the added masses are calculated through Morison et al. (1950):

$$M_{a,pile} = C_M \frac{\rho_w \pi d^2}{4} \quad (1)$$

where  $M_{a,pile}$  = added mass per unit length;  $C_M$  = coefficient of the added mass (1.0 for circular cross-sections (Sarpkaya 1975));  $\rho_w$  = water density and  $d$  = pile diameter. As Eq. (1) is limited to structures with circular cross-sections (Bhatta

and Rahman 2003), the added mass on rectangular pile-caps is calculated following Zhang et al. (2020a, 2020b):

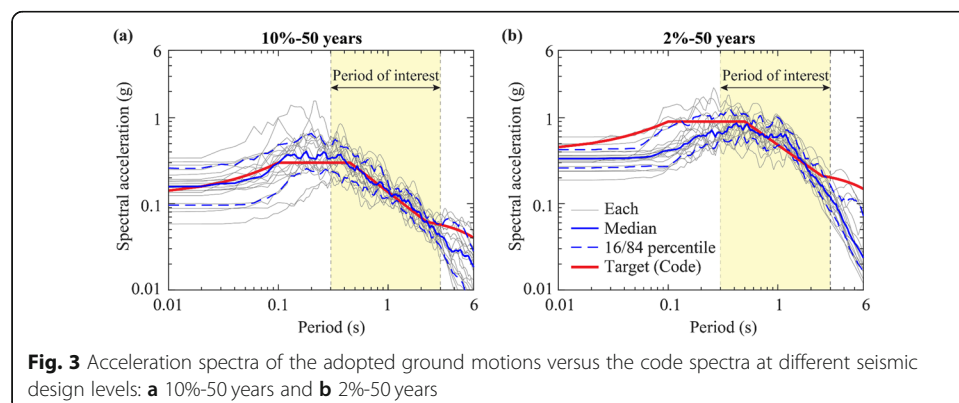
$$M_{a,cap} = 0.5742\rho_w LWH \left(\frac{L}{H}\right)^{\beta_1} \left(\frac{L}{h}\right)^{\beta_2} \left(\frac{h}{s}\right)^{\beta_3} \left(\frac{H}{h}\right)^{\beta_4} \left(\frac{W}{h}\right)^{\beta_5} \quad (2)$$

where  $L$  = the length of the pile cap (parallel to the vibration direction);  $W$  = the width of the pile cap (normal to the vibration direction);  $H$  = height of the pile-cap;  $h$  = submerged depth from the waterline to the bottom of the pile-cap and  $s$  = a parameter to determine whether the pile-cap is fully or partially submerged (i.e.  $s = H$  when  $h > H$  and  $s = h$  when  $h \leq H$ ). In this study, a fully submerged condition is considered. The exponents  $\beta_i$  ( $i = 1, 2, \dots, 5$ ) are determined based on the pile-cap dimensions, i.e.  $\beta_1 = 0.9199$ ,  $\beta_2 = -1.891$ ,  $\beta_3 = -1.1291$ ,  $\beta_4 = -0.2701\ln(H/h)$ , and  $\beta_5 = 0.2559 - 0.0771\ln(W/h)$ .

Given the dimensions of the pile-cap and piles (Fig. 2) as well as the element length of 0.5 m, the added mass for the cap is calculated as 29.23 ton (approximately 10% of the cap mass), while that for each pile-node is 0.39 ton (nearly 40% of the pile-node mass). Based on the developed soil-bridge model, the calculated added masses are imposed, from the waterline to the scoured mudlines for different cases (i.e., scour depths of 0 m, 1 m, 2 m, 3 m, 4 m, 5 m, and 6 m, as shown in Fig. 2a), to account for the hydrodynamic effect.

#### 2.4 Considered seismic design levels and selected ground motions

According to the Chinese Code for Seismic Design of Urban Bridges (MOHURD 2011) and Seismic Ground Motion Parameters Zonation Map of China (SAC 2015), two seismic hazard levels, namely 10%-50 years (i.e., return period of 475 years, denoted as “low”) and 2%-50 years (i.e., return period of 2475 years, denoted as “high”), were considered for the studied bridge at the southeast coastal region of China. The corresponding design acceleration spectra for these two hazard levels are shown in Fig. 3. To conduct nonlinear dynamic analyses under the considered seismic levels, two suites, each with 20 ground motions from earthquake events with magnitudes between 5 and 8, are selected from the Pacific Earthquake Engineering Research (PEER) Center Strong Motion Database (Ancheta et al. 2014). As can be seen in Fig. 3, the selected ground motions are scaled to be averagely compatible with the design spectra across a range of period of interest from 0.3 to 3 s, which covers the fundamental periods of the assessed bridge and soil profile (described later in this paper). Note that the scale-factors for



individual ground motions are smaller than 4 (the average scale-factor for each seismic level is smaller than 2) to avoid the overly-scaling-induced structural response biases (Watson-Lamprey and Abrahamson 2006; Davalos and Miranda 2019).

### 3 Results and discussion: influence of hydrodynamic effect across different scour depths

#### 3.1 Assessed response parameters

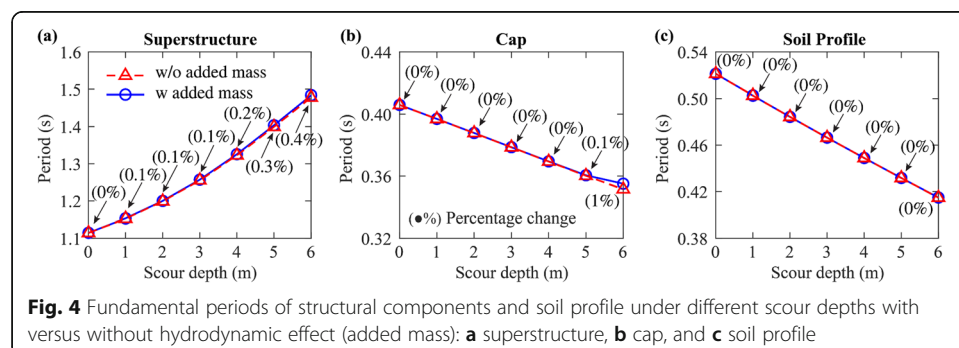
The key components of the studied bridge model, including bearing, column and pile foundation, are assessed in terms of their peak responses, i.e., peak bearing deformation, peak column curvature, and peak pile curvature. Note that the peak column curvature always occur at the bottom of the single column, while the peak pile curvature is the maximum peak one among the six piles, which is found to normally occur at the pile head of the studied bridge model.

#### 3.2 Fundamental periods of bridge components and soil profile

Before interpreting the response results, fundamental periods of the bridge components (superstructure and cap) and soil profile are presented to show the dynamic characteristics of the bridge across different scour depths, as shown in Fig. 4. The fundamental period for each component is identified through an Eigen analysis and judged according to its dominant vibration shape. The examined two cases with and without the hydrodynamic effect (i.e., with and without the added mass) are compared in terms of the percentage change:

$$\text{Percentage Change} = \frac{R_H - R_0}{R_0} \times 100\% \quad (3)$$

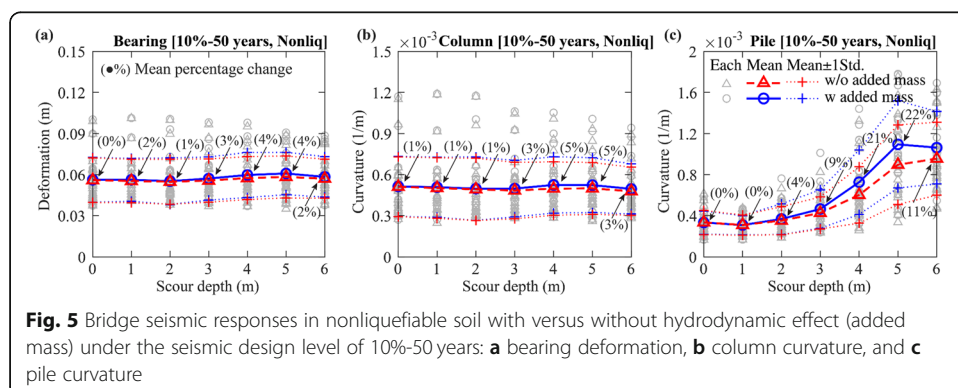
where  $R_H$  represents the case with the hydrodynamic effect, while  $R_0$  refers to the reference case that has no hydrodynamic effect. A positive percentage change indicates an increase in the result of the case with the hydrodynamic effect, while a negative percentage change means a reduction. The obtained percentage changes are marked in parentheses at individual scour depths. It is clear from Fig. 4 that the hydrodynamic effect (i.e., added mass) has almost ignorable influence on the periods (all the percentage changes are less than 1%, mostly approaching 0%), regardless of the superstructure, cap, or soil profile. More specifically, the period of the superstructure, which often represents the fundamental period of the bridge model, increases with the increasing scour depths (as seen in Fig. 4a, from nearly 1.1 s before scour to around 1.5 s under a scour



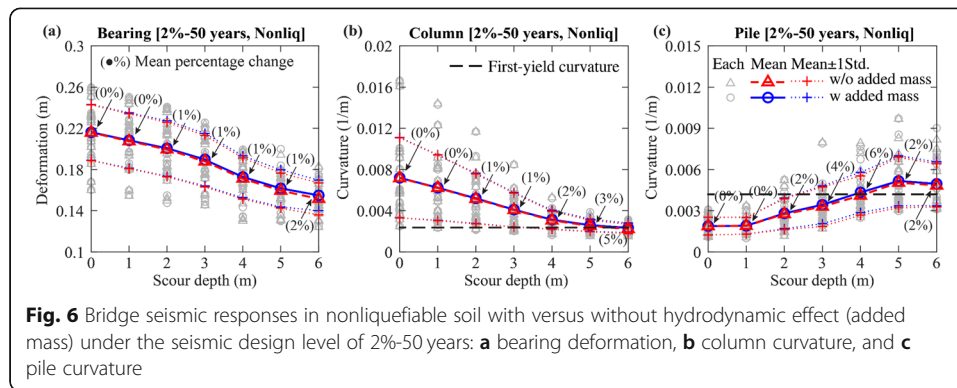
depth of 6 m). This is attributed to the fact that the increasing scour depths provide more and more flexible boundary conditions for the bridge. As for the soil profile (Fig. 4c), the period decreases along with the increase of scour depth, because the scour-induced removal of soils renders the soil column shorter, leading to a stiffer soil profile. The period of the cap (commonly the second-order structural period of the bridge) is relatively complex, which is jointly influenced by the superstructure and soil profile. In this study, it decreases with the increasing scour depths (Fig. 4b), following the trend in the soil profile.

### 3.3 Results of nonliquefiable scenario

Figures 5 and 6 show the influence of hydrodynamic effect on responses of the bridge in nonliquefiable soils across different scour depths under the considered two seismic design levels. A quick inspection of the two figures generally shows decreasing tendencies for the bearing deformation and column curvature, while an increasing tendency for the pile curvature across the scour depths from 0 m to 6 m, which implies that the role of scour hazards tends to shift the responses (and even damage positions) from the bearing and column to the pile foundation (e.g., see Figs. 6b and c where first-yield curvatures of the column and pile are plotted to highlight the shift of damage positions). In other words, the pile foundation becomes more critical in the seismic design of bridges under scour hazards. This finding generally obeys previous studies about the influence of scour hazards on seismic fragilities of highway bridges (Wang et al. 2014, 2019b; He et al. 2020). More specifically, under increasing scour depths, the decreasing tendencies for the bearing and column responses are attributed to the reduced inertial loads on the superstructure and column due to the elongated fundamental period (see Fig. 4a). As for the pile foundation, the curvature response is relatively more complex, which is controlled by the combined effects of structural inertial loads (on superstructure, column, cap, and piles) and soil-pile kinematic loads. According to the experimental study of the authors (Wang et al. 2020), scour reduces the contribution of kinematic loads on the pile curvature, while in turn relatively increases that of the inertial loads. Note that the term “contribution” means the relative role of the kinematic and inertial loads on the pile curvature. In addition, the intensity of seismic wave in a shorter soil column (with a smaller fundamental period) is expected to increase, which in turn further increases the curvature responses in piles. These complex effects together yield the





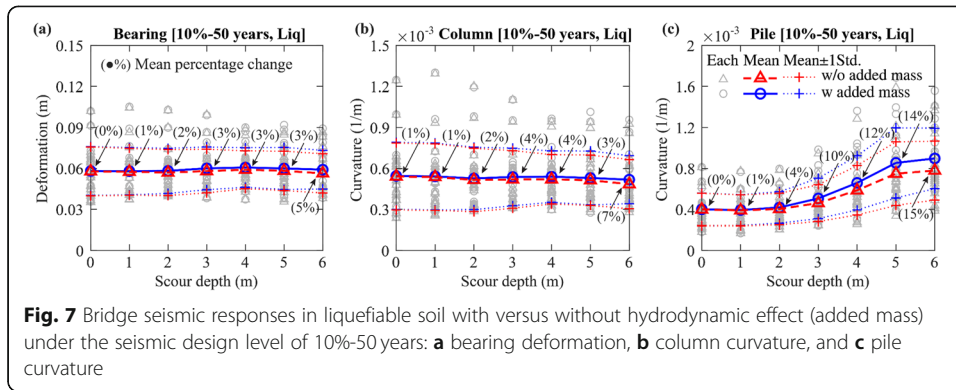


generally increasing trend of pile curvature across scour depths from 0 m to 5 m, followed by a slight decrease to the scour depth of 6 m, which indicates that 5 m tends to be an unfavorable scour depth for the studied bridge.

In terms of the quantitative influence of hydrodynamic effect on the bridge responses, different bridge components under different seismic design levels yield different results. Specifically, the bearing deformation and column curvature are slightly influenced by the hydrodynamic effect, with the percentage changes within 5% regardless under the low or high seismic design level, although the percentage changes slightly go up with the increasing scour depths (e.g., see Fig. 6b from 0% to 5% for the column curvature under the high seismic design level). This is because the bearing deformation and column curvature are primarily dependent on the inertial loads on the superstructure and column, while the hydrodynamic effect (i.e., the added inertial loads on the cap and piles) rarely contributes. As for the pile curvature response, by contrast, the hydrodynamic effect does increase the inertial loads that contribute the increase of the response. Recalling the fact that scour increases the contribution of inertial loads on pile curvature responses (Wang et al. 2020), the hydrodynamic effect is generally more noticeable under larger scour depths, as shown in Fig. 5c particularly for the low seismic design level, where the response is remarkably increased by as large as 22% at the above-identified unfavorable scour depth of 5 m. By contrast, the hydrodynamic effect-induced increase of pile curvature under the high seismic design level is significantly reduced (see Fig. 6c versus Fig. 7c). This may be because the kinematic loads under the high seismic design level dominate the pile curvature response; thereby the contribution of the additional inertial loads by the hydrodynamic effect is relatively diminished. This interpretation will be justified in the following section.

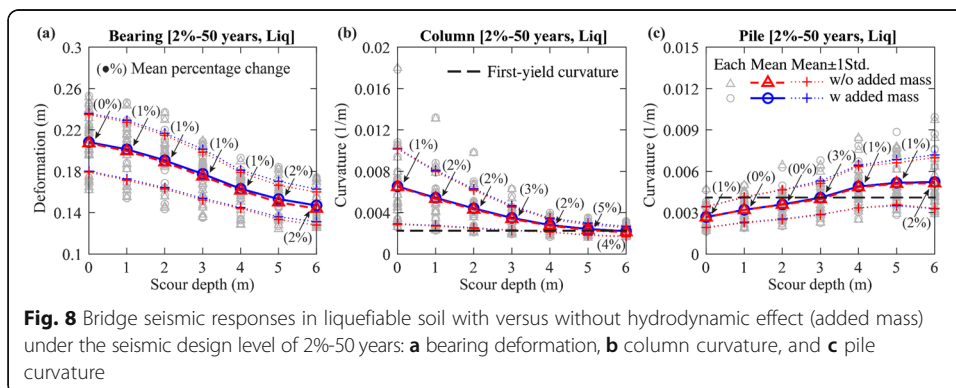
### 3.4 Results of liquefiable scenario

The influence of hydrodynamic effect on the bridge responses in liquefiable soils is shown in Figs. 7 and 8 for the low (10%-50 years) and high (2%-50 years) seismic design levels, respectively. In general, the liquefiable scenario exhibits quite similar tendencies in terms of the influence of hydrodynamic effect on the responses of different bridge components. A close inspection from Figs. 5 to 8 shows that the role of soil liquefaction



reduces the influence of hydrodynamic effect (i.e., added inertial loads) on the pile curvature, e.g., from 22% to 14% for the scour depth of 5 m under the low seismic design level (see Fig. 5c versus Fig. 7c). This can be explained by the findings from the experimental study on seismic behavior of pile-supported bridge models in liquefiable and nonliquefiable soils (Wang et al. 2019c), i.e., soil liquefaction reduces the contribution of inertial loads on pile curvature responses, while increases that of kinematic loads. Accordingly, the added inertial loads by the hydrodynamic effect cannot cause an increase of pile curvature response as remarkable as the nonliquefiable scenario. In other words, it is reasonable to infer that the increase of the contribution of kinematic loads on pile curvature responses diminishes the contribution of the additional inertial loads by the hydrodynamic effect. This inference justifies the above interpretation that the very slight influence of hydrodynamic effect on the pile curvature response under the high seismic design level is because the kinematic loads dominates the response.

Besides, it is interesting to find that uncertainties (i.e., dispersions) of the bearing deformation and column curvature responses generally decrease with the increasing scour depths, while that of the pile curvature response shows an opposite trend. This result indicates that for seismic design of bridges under scour potential, a relatively large design margin (i.e., safety factor) should be considered for the responses of bearings and columns before scour, while after scour the design margin for pile foundations should be amplified.



#### 4 Conclusions

The current paper aims to quantify the water-induced hydrodynamic effect on seismic responses of coastal highway bridges under scour and liquefaction potential. To this end, a nonlinear finite element model of a typical coastal highway bridge is established in which the hydrodynamic effect is simulated by the added mass method for both piles and cap. Two suites of 20 ground motions are selected as seismic inputs, which is compatible with two code-spectra with different hazard levels (i.e. 10%-50 years and 2%-50 years) to present two seismic design levels (i.e., low and high). Probabilistic seismic responses of different bridge components, including bearing deformation, column curvature, and pile curvature, are examined to assess the hydrodynamic effect through the relative percentage changes from the reference case without added mass to the case with added mass. The main conclusions of this study are drawn as follows.

- (1). The hydrodynamic effect has little influence on the fundamental periods of the examined soil-bridge systems under different scour depths from 0 m to 6 m. Because of this, the bearing deformation and column curvature are slightly influenced by the hydrodynamic effect, regardless of the considered scour depths and seismic design levels.
- (2). As for the pile curvature, by contrast, the hydrodynamic effect does increase the response under the low seismic design level, by as large as 15%–20% under the scour depth around 5 m in particular, whereas the hydrodynamic effect under the high seismic design level has an ignorable impact, disregarding scour depths.
- (3). The role of scour shows a tendency to shift the seismic damage position of the examined coastal highway bridge from the column to the pile foundation, regardless under the liquefiable or nonliquefiable scenario. The hydrodynamic effect does not affect this tendency. Furthermore, the dispersions of seismic responses under the adopted ground motions imply that a relatively large design margin (i.e., safety factor) is needed for bearings and columns before scour, while after scour the design margin for pile foundations should be amplified.
- (4). The role of liquefaction has ignorable impact on the influence of hydrodynamic effect on bearing deformation and column curvature. However, it diminishes the influence of hydrodynamic effect on pile curvature.

It is worth again noting that the conclusions are limited to the studied typical coastal highway bridge in cohesionless soil profiles subjected to scour depths from 0 m to 6 m. Special care should be taken when applying these conclusions to circumstances with apparent differences. Future studies will explore the quantitative contribution of inertial and kinematic loads on the studied bridges as well as use more complex finite element models to quantify the seismic responses of other bridge components such as abutments, shear keys, etc. Besides, the considered hydrodynamic effect does not cover the extreme meteorological hazards-induced breaking waves. A separate study on the influence of breaking waves will be a direction. In addition, analytical and numerical solutions to unfavorable scour depths for pile-supported bridges under scour, liquefaction, and hydrodynamic effects will be another direction.

## 5 Appendix

Tables 1 and 2 list the information of selected ground motions, including the earthquake event, magnitude ( $M_w$ ), source distance ( $R$ ), record sequence number (RSN) and adopted scaled factor, for the two seismic design levels, 10%-50 years and 2%-50 years, respectively.

**Table 1** Selected ground motions for the code-compatible spectrum representing the design level of 10%-50 years

#	Earthquake event	RSN	$M_w$	$R$ (km)	Scale factor
1	Kern County, 1952	12	7.36	117.8	1.40
2	Kern County, 1952	13	7.36	125.6	1.82
3	Kern County, 1952	15	7.36	38.9	0.87
4	Parkfield, 1966	28	6.19	17.6	2.40
5	Parkfield, 1966	30	6.19	9.6	0.68
6	Borrego Mtn, 1968	40	6.63	129.1	3.51
7	San Fernando, 1971	51	6.61	55.2	3.40
8	San Fernando, 1971	65	6.61	46.8	2.33
9	San Fernando, 1971	68	6.61	22.8	0.61
10	San Fernando, 1971	79	6.61	25.5	1.58
11	San Fernando, 1971	81	6.61	39.0	3.23
12	San Fernando, 1971	83	6.61	52.6	3.11
13	San Fernando, 1971	85	6.61	108.0	3.32
14	San Fernando, 1971	88	6.61	24.9	1.37
15	San Fernando, 1971	93	6.61	39.5	1.82
16	Managua_ Nicaragua-01, 1972	95	6.24	4.1	0.52
17	Managua_ Nicaragua-02, 1972	96	5.20	5.0	0.60
18	Friuli_ Italy-02, 1976	133	5.91	14.5	3.02
19	Tabas_ Iran, 1978	137	7.35	120.8	3.36
20	Tabas_ Iran, 1978	138	7.35	28.8	1.00

Note: RSN-Record sequence number in the PEER West2 Strong Motion Database;  $M_w$ -Magnitude;  $R$ -Source distance

**Table 2** Selected ground motions for the code-compatible spectrum representing the design level of 2%-50 years

#	Earthquake event	RSN	$M_w$	$R$ (km)	Scale factor
1	Kern County, 1952	15	7.36	38.89	2.83
2	San Fernando, 1971	68	6.61	22.77	2.24
3	San Fernando, 1971	70	6.61	27.40	2.48
4	San Fernando, 1971	78	6.61	28.99	2.73
5	Tabas_ Iran, 1978	138	7.35	28.79	3.27
6	Irpinia_ Italy, 1980	286	6.90	21.26	2.92
7	Coalinga-01, 1983	322	6.36	24.02	1.73
8	Coalinga-01, 1983	324	6.36	43.68	3.64
9	Coalinga-01, 1983	335	6.36	31.62	2.60
10	Coalinga-01, 1983	337	6.36	29.34	2.98
11	Coalinga-01, 1983	339	6.36	29.38	2.00
12	Coalinga-01, 1983	340	6.36	27.67	3.13
13	Coalinga-01, 1983	341	6.36	38.95	2.12
14	Coalinga-01, 1983	345	6.36	31.21	2.09
15	Coalinga-01, 1983	346	6.36	29.94	2.39
16	Coalinga-01, 1983	350	6.36	37.02	3.56
17	Coalinga-01, 1983	351	6.36	30.07	3.59
18	Coalinga-01, 1983	359	6.36	26.38	1.95
19	Coalinga-01, 1983	360	6.36	29.12	3.64
20	Coalinga-01, 1983	363	6.36	32.17	2.82

Note: RSN-Record sequence number in the PEER West2 Strong Motion Database;  $M_w$ -Magnitude;  $R$ -Source distance

#### Acknowledgements

Special thanks to the constructive comments by the anonymous reviewers.

#### Authors' contributions

Xiaowei Wang designed the research protocol, developed the finite element model, and wrote the manuscript draft. Yutao Pang contributed the finite element modeling in terms of calculating the added mass and selecting code-compatible ground motion records. Yutao Pang and Aijun Ye revised the manuscript and provided constructive insights. All authors read and approved the final manuscript.

#### Funding

This study is partially supported by the National Natural Science Foundation of China (52008155, 51708527 and 51778469) and the China Postdoctoral Science Foundation (2018 M640448 and 2019 T120380).

#### Availability of data and materials

The data and materials in the current study are available from the corresponding author on reasonable request.

#### Competing interests

The authors declare that they have no competing interests.

#### Author details

<sup>1</sup>College of Civil and Transportation Engineering, Hohai University, Nanjing 210024, Jiangsu, China. <sup>2</sup>Department of Civil and Environmental Engineering, Case Western Reserve University, Cleveland, OH 44106, USA. <sup>3</sup>Faculty of Engineering, China University of Geosciences (Wuhan), Wuhan 430074, Hubei, China. <sup>4</sup>Department of Bridge Engineering, Tongji University, Shanghai 200092, China.

Received: 26 November 2020 Accepted: 8 December 2020

Published online: 28 December 2020

#### References

- Alipour A, Shafei B, Shinozuka M (2012) Reliability-based calibration of load and resistance factors for design of RC bridges under multiple extreme events: scour and earthquake. *J Bridg Eng* 18(5):362–371
- Ancheta TD, Darragh RB, Stewart JP et al (2014) NGA-West2 database. *Earthquake Spectra* 30(3):989–1005
- Aygün B, Dueñas-Osorio L, Padgett JE et al (2011) Efficient longitudinal seismic fragility assessment of a multispan continuous steel bridge on liquefiable soils. *J Bridg Eng* 16(1):93–107

- Bhatta DD, Rahman M (2003) On scattering and radiation problem for a cylinder in water of finite depth. *Int J Eng Sci* 41(9): 931–967
- Biot MA (1955) Theory of elasticity and consolidation for a porous anisotropic solid. *J Appl Phys* 26(2):182–185
- Boulanger RW, Curras CJ, Kutter BL et al (1999) Seismic soil-pile-structure interaction experiments and analyses. *J Geotech Geoenviron Eng* 125(9):750–759
- Brandenberg SJ, Kashighandi P, Zhang J et al (2011) Fragility functions for bridges in liquefaction-induced lateral spreads. *Earthquake Spectra* 27(3):683–717
- Brandenberg SJ, Zhao M, Boulanger RW et al (2013) P-y plasticity model for nonlinear dynamic analysis of piles in liquefiable soil. *J Geotech Geoenviron Eng* 139(8):1262–1274
- Chen X (2020) System fragility assessment of tall-pier bridges subjected to near-fault ground motions. *J Bridg Eng* 25(3): 04019143
- Cubrinovski M, Haskell J, Winkley A et al (2014) Performance of bridges in liquefied deposits during the 2010–2011 Christchurch, New Zealand, earthquakes. *J Perform Constr Facil* 28(1):24–39
- Davalos H, Miranda E (2019) Evaluation of the scaling factor bias influence on the probability of collapse using  $S_d(T_i)$  as the intensity measure. *Earthquake Spectra* 35(2):679–702
- Di Pilato M, Feriani A, Perotti F (2008) Numerical models for the dynamic response of submerged floating tunnels under seismic loading. *Earthq Eng Struct Dyn* 37(9):1203–1222
- Filippou FC, Popov EP, Bertero WW (1983) Effects of bond deterioration on hysteretic behavior of reinforced concrete joints. In: *Earthquake Engineering Research Center, Report No. EERC 83-19*. University of California, Berkeley
- Fioklou A, Alipour A (2019) Significance of non-uniform scour on the seismic performance of bridges. *Struct Infrastruct Eng* 15(6):822–836
- Goyal A, Chopra AK (1989) Hydrodynamic and foundation interaction effects in dynamics of intake towers: earthquake responses. *J Struct Eng* 115(6):1386–1395
- Guo X, Wu Y, Guo Y (2016) Time-dependent seismic fragility analysis of bridge systems under scour hazard and earthquake loads. *Eng Struct* 121:52–60
- He H, Wei K, Zhang J et al (2020) Application of endurance time method to seismic fragility evaluation of highway bridges considering scour effect. *Soil Dyn Earthq Eng* 136:106243
- He Z, Liu W, Wang X et al (2016) Optimal force-based beam-column element size for reinforced-concrete piles in bridges. *J Bridg Eng* 21(11):06016006
- Hutchinson TC, Chai YH, Boulanger RW et al (2004) Inelastic seismic response of extended pile-shaft-supported bridge structures. *Earthquake Spectra* 20(4):1057–1080
- Jiang H, Wang B, Bai X et al (2017) Simplified expression of hydrodynamic pressure on Deepwater cylindrical bridge piers during earthquakes. *J Bridg Eng* 22(6):04017014
- Khelifa A, Garrow LA, Higgins MJ et al (2013) Impacts of climate change on scour-vulnerable bridges: assessment based on HYRISK. *J Infrastruct Syst* 19(2):138–146
- Khosravifar A, Boulanger RW, Kunnath SK (2014a) Effects of liquefaction on inelastic demands on extended pile shafts. *Earthquake Spectra* 30(4):1749–1773
- Khosravifar A, Boulanger RW, Kunnath SK (2014b) Design of extended pile shafts for the effects of liquefaction. *Earthquake Spectra* 30(4):1775–1799
- Li Q, Yang W (2013) An improved method of hydrodynamic pressure calculation for circular hollow piers in deep water under earthquake. *Ocean Eng* 72:241–256
- Liang F, Liang X, Zhang H et al (2020) Seismic response from centrifuge model tests of a scoured bridge with a pile-group foundation. *J Bridg Eng* 25(8):04020054
- Liaw CY, Chopra AK (1974) Dynamics of towers surrounded by water. *Earthq Eng Struct Dyn* 3(1):33–49
- Liu T, Wang X, Ye A (2020) Roles of pile-group and cap-rotation effects on seismic failure mechanisms of partially-embedded bridge foundations: quasi-static tests. *Soil Dyn Earthq Eng* 132:106074
- Mander JB, Priestley MJN, Park R (1988) Theoretical stress-strain model for confined concrete. *J Struct Eng* 114(8): 1804–1826
- McKenna F, Scott MH, Fenves GL (2010) Nonlinear finite-element analysis software architecture using object composition. *J Comput Civ Eng* 24(1):95–107
- Mohanty P, Dutta SC, Bhattacharya S (2017) Proposed mechanism for mid-span failure of pile supported river bridges during seismic liquefaction. *Soil Dyn Earthq Eng* 102:41–45
- MOHURD (2011) Code for seismic Design of Urban Bridges, Ministry of Housing and Urban-Rural Development of China, Beijing
- Mokwa RL (1999) Investigation of the resistance of pile caps to lateral loading Virginia Tech
- Morison JR, Johnson JW, Schaaf SA (1950) The force exerted by surface waves on piles. *J Pet Technol* 2(5):149–154
- Olson LG, Bathe KJ (1985) Analysis of fluid-structure interactions. A direct symmetric coupled formulation based on the fluid velocity potential. *Comput Struct* 21(1–2):21–32
- Padgett JE, Ghosh J, Dueñas-Osorio L (2010) Effects of liquefiable soil and bridge modelling parameters on the seismic reliability of critical structural components. *Struct Infrastruct Eng* 9(1):59–77
- Padgett JE, Spiller A, Arnold C (2012) Statistical analysis of coastal bridge vulnerability based on empirical evidence from hurricane Katrina. *Struct Infrastruct Eng* 8(6):595–605
- Pang Y, Cai L, He W et al (2020) Seismic assessment of deep water bridges in reservoir considering hydrodynamic effects using endurance time analysis. *Ocean Eng* 198:106846
- Pang Y, Kai W, Yuan W et al (2015) Effects of dynamic fluid-structure interaction on seismic response of multi-span deep water bridges using fragility function method. *Adv Struct Eng* 18(4):525–542
- Robertson IN, Yim S, Riggs HR et al (2007) Coastal bridge performance during hurricane Katrina. In: Zingoni A (ed) *Third international conference on structural engineering, mechanics and computation, SEMC-2007*. Cape Town, South Africa, pp 1864–1870
- SAC (2015) Seismic ground motion parameters zonation map of China. Standardization Administration of China, Beijing
- Sarpkaya T (1975) Forces on cylinders and spheres in a sinusoidally oscillating fluid. *J Appl Mech* 42(1):32–37

- Song S, Hu T, Chiou D (2020) Influence of riverbed scour on the performance of bridges subjected to lateral seismic loads. *J Earthq Eng* 00(00):1–32
- Su L, Lu J, Elgamal A et al (2017) Seismic performance of a pile-supported wharf: three-dimensional finite element simulation. *Soil Dyn Earthq Eng* 95:167–179
- Wang P, Zhao M, Du X (2019) A simple added mass model for simulating elliptical cylinder vibrating in water under earthquake action. *Ocean Eng* 179:351–360
- Wang R, Liu X, Zhang JM (2017a) Numerical analysis of the seismic inertial and kinematic effects on pile bending moment in liquefiable soils. *Acta Geotech* 12(4):773–791
- Wang X, Ji B, Ye A (2020) Seismic behavior of pile-group-supported bridges in liquefiable soils with crusts subjected to potential scour: insights from shake-table tests. *J Geotech Geoenviron Eng* 146(5):04020030
- Wang X, Luo F, Su Z et al (2017b) Efficient finite-element model for seismic response estimation of piles and soils in liquefied and laterally spreading ground considering shear localization. *Int J Geomech* 17(6):06016039
- Wang X, Shafieezadeh A, Ye A (2018) Optimal intensity measures for probabilistic seismic demand modeling of extended pile-shaft-supported bridges in liquefied and laterally spreading ground. *Bull Earthq Eng* 16(1):229–257
- Wang X, Shafieezadeh A, Ye A (2019a) Optimal EDPs for post-earthquake damage assessment of extended pile-shaft-supported bridges subjected to transverse spreading. *Earthquake Spectra* 35(3):1367–1396
- Wang X, Ye A, Ji B (2019b) Fragility-based sensitivity analysis on the seismic performance of pile-group-supported bridges in liquefiable ground undergoing scour potentials. *Eng Struct* 198:109427
- Wang X, Ye A, Shang Y et al (2019c) Shake-table investigation of scoured RC pile-group-supported bridges in liquefiable and nonliquefiable soils. *Earthq Eng Struct Dyn* 48(11):1217–1237
- Wang Z, Dueñas-Osorio L, Padgett JE (2014) Influence of scour effects on the seismic response of reinforced concrete bridges. *Eng Struct* 76:202–214
- Watson-Lamprey J, Abrahamson N (2006) Selection of ground motion time series and limits on scaling. *Soil Dyn Earthq Eng* 26(5):477–482
- Wei K, Yuan W, Bouaanani N (2013) Experimental and numerical assessment of the three-dimensional modal dynamic response of bridge pile foundations submerged in water. *J Bridg Eng* 18(10):1032–1041
- Westergaard HM (1933) Water pressures on dams during earthquakes. *Trans* 98:418–433
- Xie Y, Zhang J, Huo Y (2018) Simplified drift demand prediction of bridges under liquefaction-induced lateral spreading. *J Bridg Eng* 23(8):04018053
- Yang DY, Frangopol DM (2019) Physics-based assessment of climate change impact on long-term regional bridge scour risk using hydrologic modeling: application to Lehigh River watershed. *J Bridg Eng* 24(11):04019099
- Yang Z (2000) Numerical modeling of earthquake site response including dilation and liquefaction. PhD dissertation, Columbia University
- Zhang J, Huo Y (2009) Evaluating effectiveness and optimum design of isolation devices for highway bridges using the fragility function method. *Eng Struct* 31(8):1648–1660
- Zhang J, Wei K, Pang Y et al (2019) Numerical investigation into hydrodynamic effects on the seismic response of complex hollow bridge pier submerged in reservoir. *J Bridg Eng* 24(2):05018016
- Zhang J, Wei K, Qin S (2020b) Bayesian updating model for structural vibration-induced hydrodynamic added mass of rectangular pile cap submerged in water. *J Eng Mech* 146(9):04020096
- Zhang X, Tang L, Li X et al (2020a) Effect of the combined action of lateral load and axial load on the pile instability in liquefiable soils. *Eng Struct* 205:110074
- Zhang Y, Conte JP, Yang Z et al (2008) Two-dimensional nonlinear earthquake response analysis of a bridge-foundation-ground system. *Earthquake Spectra* 24(2):343–386
- Zhong J, Jeon JS, Shao YH et al (2019) Optimal intensity measures in probabilistic seismic demand models of cable-stayed bridges subjected to pulse-like ground motions. *J Bridg Eng* 24(2):04018118
- Zhong J, Jiang L, Pang Y et al (2020) Near-fault seismic risk assessment of simply supported bridges. *Earthquake Spectra* 36(4):1645–1669

## Publisher's Note

Springer Nature remains neutral with regard to jurisdictional claims in published maps and institutional affiliations.

**Submit your manuscript to a SpringerOpen<sup>®</sup> journal and benefit from:**

- Convenient online submission
- Rigorous peer review
- Open access: articles freely available online
- High visibility within the field
- Retaining the copyright to your article

---

Submit your next manuscript at ► [springeropen.com](https://www.springeropen.com)

---